Chemical Engineering Research and Design 228 (2026) 279–289

Contents lists available at ScienceDirect

Chemical Engineering Research and Design

journal homepage: www.elsevier.com/locate/cherd

# Maximising $CO_2$ sequestration via simultaneous milling and carbonation of steel slag: A Taguchi-driven optimisation approach

Nina Miladinović [a], Luka Ceyssens [a], Giuseppe Granata [a,b], Tom Van Gerven [a,*]

[a] Process Engineering for Sustainable Systems (ProcESS), Department of Chemical Engineering, KU Leuven, Celestijnenlaan 200F, Leuven 3001, Belgium
[b] Sustainable Materials Processing and Recycling (SeMPeR), Department of Materials Engineering, KU Leuven, Vesaliusstraat 13, Leuven 3000, Belgium

ARTICLE INFO

*Keywords:*
Planetary ball mill
Mechanochemistry
Carbonation
Steel slags
Argon oxygen decarburisation (AOD) slag
Basic oxygen furnace (BOF) slag

ABSTRACT

Steel slags, byproducts of the steelmaking industry, pose a significant environmental burden due to their large volume and limited reuse opportunities. $CO_2$ sequestration represents a promising utilisation route, enabled by their diverse mineral composition. However, conventional carbonation methods are often slow and require rigorous conditions. This study presents a rapid and intensified approach for carbon capture via simultaneous milling and carbonation of basic oxygen furnace (BOF) and argon oxygen decarburisation (AOD) slags in the planetary ball mill. To optimise this complex process, a Taguchi design of experiments was employed, enabling the identification of key parameters for maximising $CO_2$ uptake. Optimal conditions, determined through signal-to-noise analysis and heatmaps, were found to be material-specific. Moreover, $CO_2$ uptake rates of 0.32 g $CO_2$/g (AOD) and 0.25 g $CO_2$/g (BOF) were achieved in just 6–8 min, meeting or exceeding values reported in the literature to date, 0.386 g $CO_2$/g (AOD) and 0.188 g $CO_2$/g (BOF) (Zhao Q. et al., 2025) (Santos M.R. et al., 2013). These results were obtained at impact energies of 110 J/g (AOD) and 152 J/g (BOF), demonstrating the system's transferability across different mills, without the leaching of harmful metals. This work highlights a time-efficient and environmentally safe method for transforming steel slags into valuable carbon sinks.

## 1. Introduction

Steel slag is a solid waste which is created in the process of steel making and is mainly composed of silica, calcium oxide, magnesium oxide, aluminium and iron oxides (Xu et al., 2017). Steel industry accounts for approximately 5% of total $CO_2$ emissions in the EU and around 7% globally (Joint Research Centre European Commission, 2022). According to the World Steel Association, more than 400 million tonnes of iron and steel slag are produced annually (World Steel Association, 2025), making the utilisation of this waste an increasing problem. Recently, steel slags have found new applications due to their chemical and physical properties, rather than being discarded as waste. They are being used as concrete aggregates, cement ingredients, mechanomutable asphalt binders or even as building materials (Dhoble and Ahmed, 2018). Other avenues for utilising slag include landfill daily cover material, water treatment, recovery of minerals and heavy metals from slag, as well as carbon sequestration (Ukwattage et al., 2017; Kim et al., 2016). Carbon sequestration represents a process of capturing and long-term storing of $CO_2$ in a stable state (Bernoux et al., 2005). This process can be direct or indirect, and of different nature, with biological, chemical, physical or geological processes involved (Jat et al., 2022). Steel slag contributes to carbon sequestration by reacting with carbon dioxide to form stable carbonates, thereby mitigating greenhouse gas emissions while also immobilising the leaching of heavy metals, which has a significant environmental impact (Biava et al., 2024). Carbonation of slag can be done through gas-solid carbonation or gas-liquid-solid carbonation. A detailed mechanism of gas-liquid-solid carbonation is presented (Digiovanni et al., 2024).

Once $CO_2$ is introduced into the aqueous environment, the reactions given in Eqs. 1 and 2 take place.

$$CO_{2(g)} \rightleftarrows CO_{2(aq)} \tag{1}$$

$$CO_{2(aq)} + H_2O_{(l)} \rightleftarrows H_2CO_{3(aq)} \rightleftarrows H^+_{(aq)} + HCO^-_{3(aq)} \rightleftarrows 2H^+_{(aq)} + CO^{2-}_{3(aq)} \tag{2}$$

In parallel, minerals from steel slag dissolve following the reaction described in Eq. 3.

$$Ca(Mg)_2SiO_{4(s)} + 4H^+_{(aq)} \rightarrow 2Ca(Mg)^{2+}_{(aq)} + SiO_{2(s)} + 2H_2O_{(l)} \tag{3}$$

In this way, calcium or magnesium ions react with carbonate ions,

* Corresponding author.
*E-mail address:* tom.vangerven@kuleuven.be (T. Van Gerven).

https://doi.org/10.1016/j.cherd.2026.02.058
Received 15 December 2025; Received in revised form 23 January 2026; Accepted 25 February 2026
Available online 26 February 2026
0263-8762/© 2026 The Author(s). Published by Elsevier Ltd on behalf of Institution of Chemical Engineers. This is an open access article under the CC BY license (http://creativecommons.org/licenses/by/4.0/).

forming carbonates as shown in Eq. 4.

$$Ca(Mg)^{2+}_{(aq)} + CO^{2-}_{3(aq)} \rightarrow Ca(Mg)CO_{3(s)} \quad (4)$$

As steel slags consist of a variety of minerals, certain phases, such as hydraulic calcium silicate phases ($Ca_3SiO_5$), undergo a hydration reaction upon contact with water and form calcium silicate hydrate ($CaO \bullet SiO_2 \bullet H_2O$ or C-S-H) and calcium hydroxide ($Ca(OH)_2$ or CH). This can be seen in Eqs. 5–7 (Goodbrake et al., 1979).

$$Ca_3SiO_{5(s)} + H_2O_{(l)} + 2CO_{2(aq)} \rightarrow CaO \bullet SiO_2 \bullet H_2O_{(s)} + 2CaCO_{3(s)} \quad (5)$$

$$3CaO \bullet 2SiO_2 \bullet 4H_2O_{(s)} + 3CO_{2(aq)} \rightarrow 3CaCO_{3(s)} + 2(SiO_2 \bullet H_2O) + 2H_2O_{(l)} \quad (6)$$

$$Ca(OH)_{2(s)} + CO_{2(aq)} \rightarrow CaCO_{3(s)} + H_2O_{(l)} \quad (7)$$

It is important to emphasise that carbonation and hydration reactions do not occur simultaneously and depend on the $CO_2$ concentration in the aqueous solution (Castellote and Andrade, 2008).

As previously noted, steel slags contain a diverse range of minerals due to the nature of their production process. Particular attention will be devoted to Basic Oxygen Furnace (BOF) and Argon Oxygen Decarburisation (AOD) slags. BOF slag is a by-product of a process in which pig iron, steel scrap and burnt lime are used, while pure oxygen is blown into the mixture (Ruth, 2004). On the other hand, AOD slag is created after the initial melting of the metal in an electric arc furnace, where it is subjected to three steps such as decarburisation, reduction and desulfurization (Krivsky, 1973). In the process of decarburisation, high-carbon ferro-chrome is added and blowing of inert gas (argon, nitrogen) and oxygen mixture is started. The reduction step essentially serves to reduce chromium oxides and depends on multiple factors (Wei et al., 2022). In the final stage, sulphur levels are adjusted to remain within a specified range, completing the desulfurization process.

According to the World Steel Association, around 1.9 billion tonnes of crude steel were produced in 2023 (World Steel Association, 2025), which approximately generates 126 kg of slag of the basic oxygen furnace route for each tonne of produced steel, and 169 kg of slag of the electric arc furnace route (World Steel Association, 2021).

High output of slags per tonne of crude steel leads to the exploration of the carbon sequestration ability of these slags. Up to the current knowledge, up to 188 g of $CO_2$ per kg of BOF slag was captured (Zhao et al., 2025) or even up to 386 g of $CO_2$ per kg of AOD slag (Santos et al., 2013). However, these rates were achieved either with very high pressures or temperatures, or with the insertion of specific additives. The common parameter was also a prolonged carbonation time, which was always above 60 min (Wang et al., 2024).

In order to accelerate the carbonation process, mechanical activation of slag is employed as a time-efficient method that can achieve comparable or even higher carbonation rates. While this method cannot be directly compared with reactor designs employed in other studies, the highest carbonation rates achieved in other systems are included for benchmarking purposes. Mechanical activation is a physicochemical change of a solid by grinding or ball milling, which contributes to the reduction of particle size but also disrupts the crystalline structure, making the material more amorphous (Zhang and Ling, 2020). In the context of mineral carbonation, mechanical activation enhances this chemical reaction, thereby classifying the process as mechanochemical. Conventionally reported parameters in terms of milling are time, applied speed, and the size/nature of the milling beads (Jafter et al., 2024). Additionally, commonly reported parameters for carbonation are time of reaction, pressure and purity of the introduced gas, and temperature of the surrounding atmosphere (Chen et al., 2021). However, these parameters are specific to a given system and their transfer between systems was shown to be unapplicable (Kremer et al., 2022). Therefore, energy supplied to the material is considered to be a better parameter for comparing the results of simultaneous milling and carbonation between different mills and for scaling it up. As previously seen, the planetary ball mill device itself consumes a high amount of energy (Miladinović et al., 2025). Nevertheless, with the implementation of the collision model theory, it is possible to estimate the power supplied to the material in this kind of mill (Magini et al., 1998). Advantages of the process of simultaneous milling and carbonation are breaking the unreacted core and exposing it to the liquid film, so that the reacting surface of a material is increased (Chalouati et al., 2023). The main disadvantage of this type of process remains to be agglomeration of certain materials due to the presence of water, as well as higher energy consumption by the equipment (Miladinović et al., 2025). The rotational speed of a mill should be calculated in order to reduce energy demands, obtain minimal agglomeration and still be able to break a particle to increase the reaction rate. This optimal rotational speed is known as the critical speed (CS) and corresponds to the minimum speed at which the milling medium is centrifugally rotated inside a jar to its full extent (Paneva et al., 2024). Besides rotational speed, parameters that can be varied in the planetary ball mill are solid-to-beads ratio, beads size, solid-to-liquid ratio, milling time, and, in case of introducing a gaseous phase - pressure and concentration of introduced gas (Pohshna and Mailapalli, 2023; De Schutter et al., 2024).

Therefore, this paper investigates energy- and time-efficient simultaneous milling and carbonation of two aforementioned slags: AOD and BOF, in the planetary ball mill. To evaluate the influence of key variables such as pressure of a gaseous phase, size of milling media, ratio of milling media and water to the material, as well as time of the process, a Taguchi experimental design is employed. Impact of these parameters on the carbonation rate of slags and observed changes in slags'

**Table 1**
Chemical composition of AOD and BOF slags presented in equivalent oxide form, obtained by WD-XRF.

| Compound | wt% in AOD | wt% in BOF |
|---|---|---|
| CaO | 57.8 | 60.4 |
| $Fe_2O_3$ | 0.17 | 19.1 |
| $SiO_2$ | 27.9 | 12.6 |
| MgO | 9.92 | 1.51 |
| MnO | 0.34 | 2.16 |
| $Al_2O_3$ | 1.74 | 1.37 |
| $Cr_2O_3$ | 0.57 | 0.15 |
| Other compounds | 1.56 | 2.71 |

**Table 2**
Mineralogical composition of AOD and BOF slags determined by XRD (minerals not present are denoted by "/").

| Mineral | PDF cards | Formula | wt% in AOD | wt% in BOF |
|---|---|---|---|---|
| Bredigite | 00–036–0399 | $Ca_7Mg(SiO_4)_4$ | 13.3 | 7.20 |
| Cuspidine | 00–041–1474 | $Ca_4Si_2O_7F_2$ | 3.54 | / |
| Merwinite | 00–035–0591 | $Ca_3Mg(SiO_4)_2$ | 48.6 | / |
| β-$C_2S$ | 00–009–0351 | $Ca_2SiO_4$ | 3.10 | 8.21 |
| γ-$C_2S$ | 00–033–0302 | $Ca_2SiO_4$ | 13.2 | / |
| Akermanite | 01–082–3035 | $Ca_2MgSi_2O_7$ | 1.75 | / |
| Srebrodolskite | 00–047–1744 | $Ca_2Fe_2O_5$ | / | 15.3 |
| Wollastonite | 04–010–2581 | $CaSiO_3$ | 1.10 | / |
| Portlandite | 00–044–1481 | $Ca(OH)_2$ | / | 10.8 |
| Fluorite | 00–035–0816 | $CaF_2$ | 3.24 | / |
| Magnetite | 04–023–1463 | $Fe_3O_4$ | / | 2.94 |
| Haematite | 00–033–0664 | $Fe_2O_3$ | / | 0.69 |
| Wustite | 00–006–0615 | FeO | / | 4.86 |
| Iron | 00–006–0696 | Fe | / | 0.31 |
| Periclase | 00–043–1022 | MgO | 3.55 | 3.08 |
| Quartz | 00–033–0256 | $SiO_2$ | 0.69 | 1.45 |
| Calcite | 04–008–0198 | $CaCO_3$ | 2.23 | 3.34 |
| Amorphous phase | / | / | 5.70 | 41.8 |

**Table 3**
Varied parameters distributed in L16b orthogonal array.

| Run | Pressure [bar] | Bead size [mm] | Slag: bead ratio [1 g: x g] | Slag: water ratio [1 g: x g] | Time [min] |
|---|---|---|---|---|---|
| 1 | 1 | 2 | 10 | 5 | 2 |
| 2 | 1 | 3 | 20 | 10 | 4 |
| 3 | 1 | 5 | 30 | 15 | 6 |
| 4 | 1 | 10 | 40 | 20 | 8 |
| 5 | 2 | 2 | 20 | 15 | 8 |
| 6 | 2 | 3 | 10 | 20 | 6 |
| 7 | 2 | 5 | 40 | 5 | 4 |
| 8 | 2 | 10 | 30 | 10 | 2 |
| 9 | 4 | 2 | 30 | 20 | 4 |
| 10 | 4 | 3 | 40 | 15 | 2 |
| 11 | 4 | 5 | 10 | 10 | 8 |
| 12 | 4 | 10 | 20 | 5 | 6 |
| 13 | 5 | 2 | 40 | 10 | 6 |
| 14 | 5 | 3 | 30 | 5 | 8 |
| 15 | 5 | 5 | 20 | 20 | 2 |
| 16 | 5 | 10 | 10 | 15 | 4 |

mineralogy are examined.

## 2. Materials and methods

### 2.1. Characterisation of steel slags

Received slags were characterised using Wavelength Dispersive X-ray fluorescence spectroscopy (WD-XRF) on *Bruker* S8 TIGER 4 kW with the glass beads method and X-ray powder diffraction (XRD) on Aeris *Malvern Panalytical* and CuKα radiation at 15 mA and 40 kV with 2θ ranging 5–70°. Data obtained by these techniques are given in Tables 1 and 2 for WD-XRF and XRD, respectively. The morphology of slags is observed using Scanning Electron Microscopy (SEM) *Tescan Mira.* Samples were prepared by dispersing slags onto stubs with conductive carbon tape and coated with a 5 nm Pt/Pd coating.

### 2.2. Taguchi design of experiments

The Taguchi method for experimental design is one of the most effective techniques for reducing the number of trials (Hisam et al., 2024). This method is based on controlling parameters in a way that reduces variability in the response variable and achieves the target level (Mitra, 2011). For this purpose, an orthogonal array distribution of factors is used, where variables are distributed in a balanced manner, and their effect on the response can easily be analysed (Morsi et al., 2004). In this research, the L16b orthogonal array with five four-level factors is used (University Of York, 2004). Detailed design is given in Table 3. All experiments are performed in triplicate in the planetary ball mill Planetary Micro Mill PULVERISETTE 7 premium line, *Fritsch,* at ambient temperature.

As seen in Table 3, the five varied parameters are pressure of 99.9% $CO_2$ injected on top of a grinding bowl, bead size of zirconium milling media, slag-to-bead ratio, slag-to-water ratio and time of simultaneous milling and carbonation. Levels of these factors were selected based on previous research, which demonstrated that satisfactory carbonation results are obtained when all factors are simultaneously applied at their highest levels (Miladinović et al., 2025; De Schutter et al., 2024). Therefore, three lower levels for each parameter are chosen to find the optimal parameters at the lowest possible level. Moreover, it is worth noting that the $CO_2$ pressure of 5 bar was selected due to a technical limitation of the system, as the grinding bowls are certified for operation up to 5.5 bar.

The critical rotational speed (CS) of a planetary ball mill is defined as the minimum speed to achieve maximum mechanical activation for a given planetary ball mill and a given bead diameter. It can be determined using Eq. 8 (Odebiyi et al., 2024), yielding in this case a value of 230 rpm (24 rad/s).

$$CS = \frac{1}{2\pi}\sqrt{\frac{g}{R-r}} \tag{8}$$

Where $R$ represents the radius of a mill used [m], $g$ represents the acceleration due to gravity (9.81 $\frac{m}{s^2}$) and $r$ represents the radius of the beads used [m].

To incorporate a safety margin, a slightly higher speed of 250 rpm was employed. Experimental underpinning of these calculations for AOD and BOF are given in Supplementary data Figs. 1a and 1b, respectively.

### 2.3. $CO_2$ uptake

The experimental uptake of $CO_2$ is determined using the RW-24 Enhanced Rock Weathering calcimeter (BD Inventions). The working principle of this device is based on the Scheibler method (ISO 10693:1995). Results obtained by this method are confirmed with X-ray powder diffraction (XRD). Samples analysed with XRD are milled together with 10 wt% of corundum as an internal standard and ethanol in a McCrone micronising mill. Mineral phases were identified using Bruker DIFFRAC.EVA software and the quantification were performed by Rietveld refinement on Topas 6 Academic (Alan Coelho). Eq. 9 is used to estimate $CO_2$ uptake based on calcium carbonate content measured by both methods.

$$CO_2\ uptake = \frac{M(CO_2) \times w\%CaCO_3}{M(CaCO_3)} \tag{9}$$

Where $M(CO_2)$ represents the molar mass of carbon dioxide, $w\%CaCO_3$ denotes the weight percent of calcium carbonate present, and $M(CaCO_3)$ is the molar mass of calcium carbonate.

### 2.4. Examination of leaching and particle size

Leaching of elements in the water during the process of simultaneous milling and carbonation is examined using inductively coupled plasma optical emission spectroscopy (ICP-OES) on Optima 8300 *PerkinElmer*. Samples were diluted in 2 vol% nitric acid with lutetium as an internal standard. The particle size of the material after simultaneous milling and carbonation is determined using a laser particle size analyser, Mastersizer 3000 – Hydro EV, *Malvern Panalytical.* The material was dispersed in absolute ethanol (*Fisher Scientific B.V.*, Belgium) with the obscuration rate of 10–20% mass fraction.

### 2.5. Analysis of data obtained by Taguchi design of experiments

Carbon dioxide uptake obtained from experimental runs is analysed using two different approaches. One approach was using the signal-to-noise (S/N) ratio. This ratio is used to evaluate the quality of an outcome by comparing the desired signal with the noise or unwanted variation in the output (Rashid, 2023). In this research, the larger-the-better S/N ratio (Eq. 10) was used, as $CO_2$ uptake should be maximised (Madu and Madu, 1999). The parameter level that corresponds to the highest S/N ratio is considered the optimal level for that parameter (Radune et al., 2022).

$$S/N = -10 \times \log\frac{\sum\frac{1}{Y^2}}{n} \tag{10}$$

Where $n$ is the number of repetitions of the same experiment, and $Y$ is the result of the experiment – in this case, the achieved carbonation rate.

The second approach involved maximising mean $CO_2$ uptake through the use of heatmaps, where the maximum average carbonation rate per factor was normalised to 1 and the minimum average

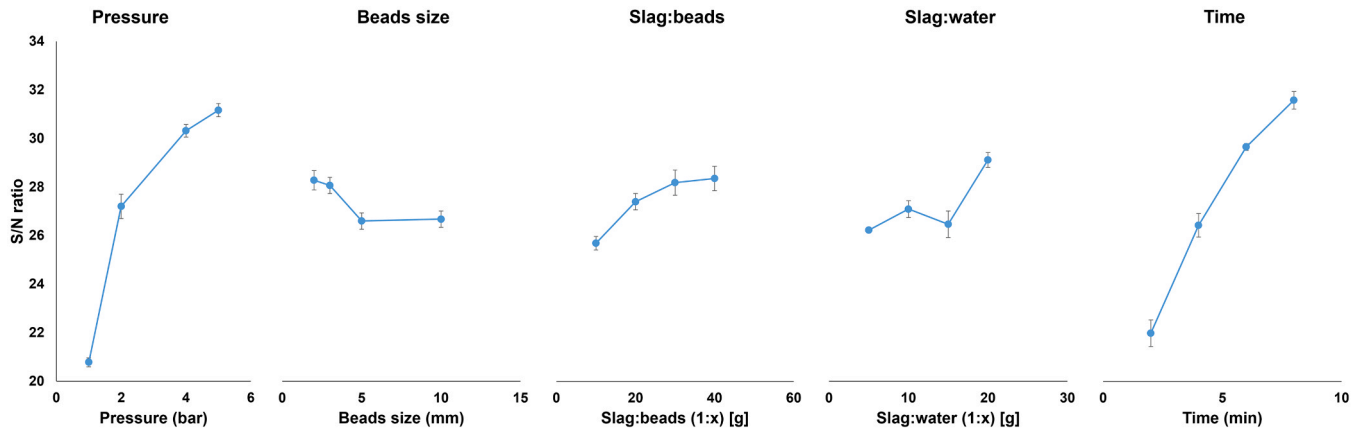



**Fig. 1.** Impact of various parameters on S/N ratio for AOD slag based on the DOE given in L16b orthogonal array.

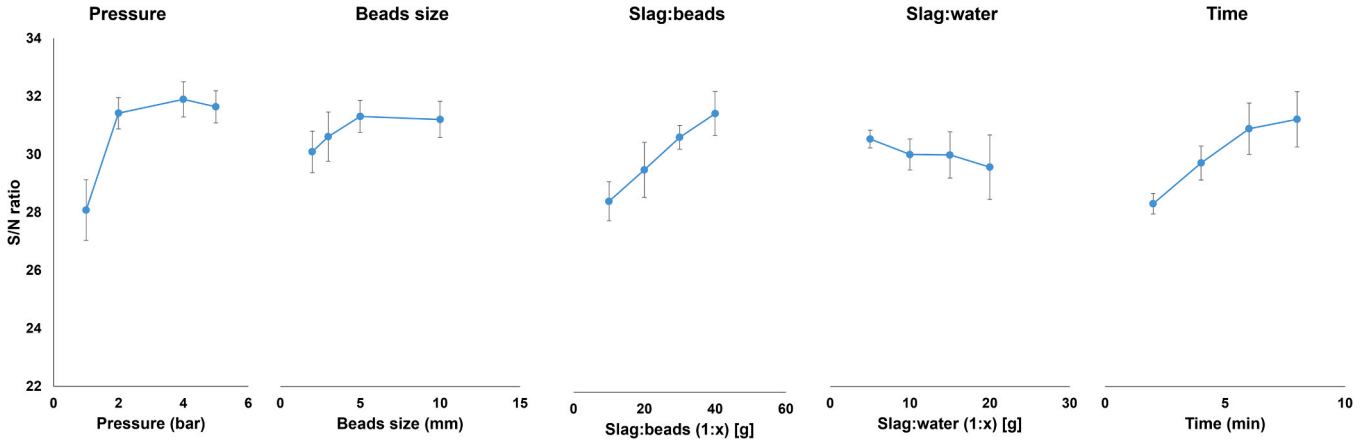



**Fig. 2.** Impact of various parameters on S/N ratio for BOF slag based on the DOE given in L16b orthogonal array.

carbonation rate per factor was normalised to 0. Based on these calculations, other values were assigned corresponding numbers between 0 and 1, resulting in the formation of a heatmap. Additionally, analysis of variance (ANOVA) is done in order to determine the percentage contribution of each factor on carbon dioxide uptake (Ståhle and Wold, 1989).

### 2.6. Impact energy

For calculating the impact energy of materials based on the type of mill and the parameters employed, Eq. 11 is used (Khoa et al., 2004).

$$E = \frac{1}{2} K_a K_b K_v m_b W_p^3 R_p^2 N_b t \quad (11)$$

Where $K_a$ is a constant depending on the type of collision ($K_a = 1$), $K_b$ is a constant depending on the geometry of the mill ($K_b = 1.06$), and $K_v$ is a constant that depends on the reaction kinetics ($K_v = 0.35$) . (Khoa et al., 2004) $m_b$ is the average mass of one bead [kg], while $W_p$ is the rotational speed of the disk [rad/s] and $R_p$ is the distance between the axis of a bowl and the disk of a mill [m]. $N_b$ is a number of grinding beads, and $t$ is time [s].

## 3. Results and discussion

### 3.1. Impact of varied parameters on $CO_2$ uptake

#### 3.1.1. Signal-to-noise (S/N) ratio

The influence of five different parameters on the S/N ratio based on the carbonation rate achieved during simultaneous milling and carbonation in the planetary ball mill is shown for AOD and BOF in Figs. 1 and 2, respectively. Carbonation rates obtained in each experimental run, analysed with a calcimeter and XRD, can be seen in Supplementary data Table 1.

Fig. 1 illustrates that pressure plays a crucial role in the carbonation process of AOD. The higher the applied pressure, the higher the S/N ratio, which indicates increased carbonation rates. Several factors can influence this behaviour. Firstly, an increase in pressure enhances the dissolution of gases, specifically carbon dioxide. Secondly, since carbonation occurs concurrently with milling, high pressure, in addition to the mechanical activation, promotes the amorphisation of the material due to lower bulk densities of the amorphous phase than its crystalline counterparts, leading to improved carbonation (Arora, 2000; Cui et al., 2019). This trend was particularly evident for AOD slag as indicated by the XRD results shown in Supplementary data Table 2. Therefore, it can be concluded that higher pressures are more suitable for AOD slag in this system. Regarding bead size, smaller beads (2 mm and 3 mm) yield slightly better results than larger beads (5 mm and 10 mm), likely due to the finer nature of the raw material, as the AOD slag initially has a mean particle diameter of 44 μm. This phenomenon occurs due to the fact that smaller beads increase the surface area contact between the beads and the material being milled, leading to more efficient grinding and dispersion of fine particles (Z-Mixer, 2025). Additionally, increasing the slag-to-bead ratio improves performance, though beyond a ratio of 1:30 g/g, carbonation rate reaches a plateau, indicating only slight improvement. The slag-to-water ratio shows a slight impact at higher ratios, most likely due to a leaching effect that

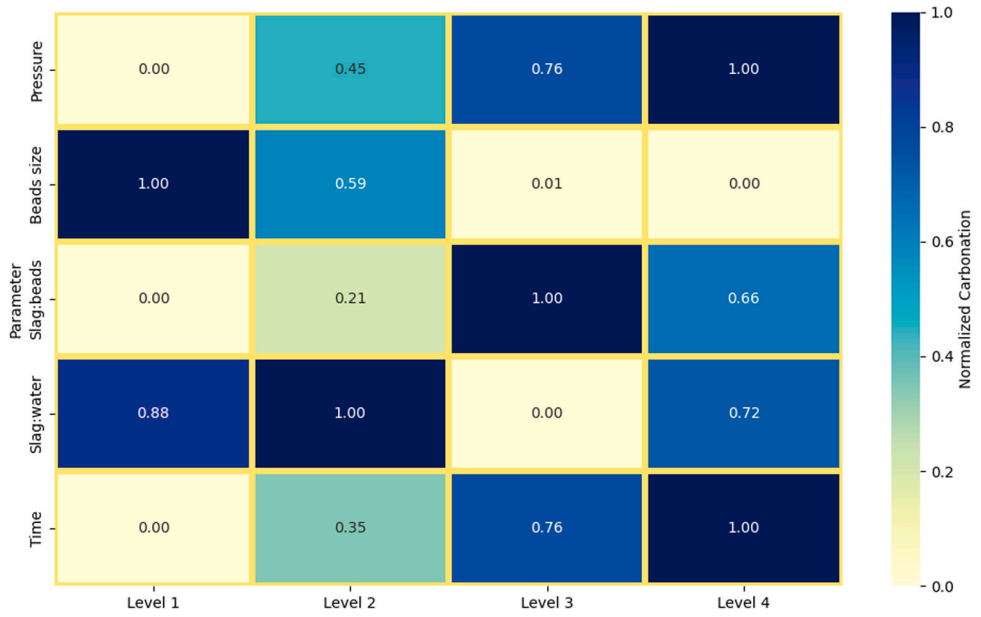



**Fig. 3.** Impact of various parameters on carbonation rate for AOD slag.

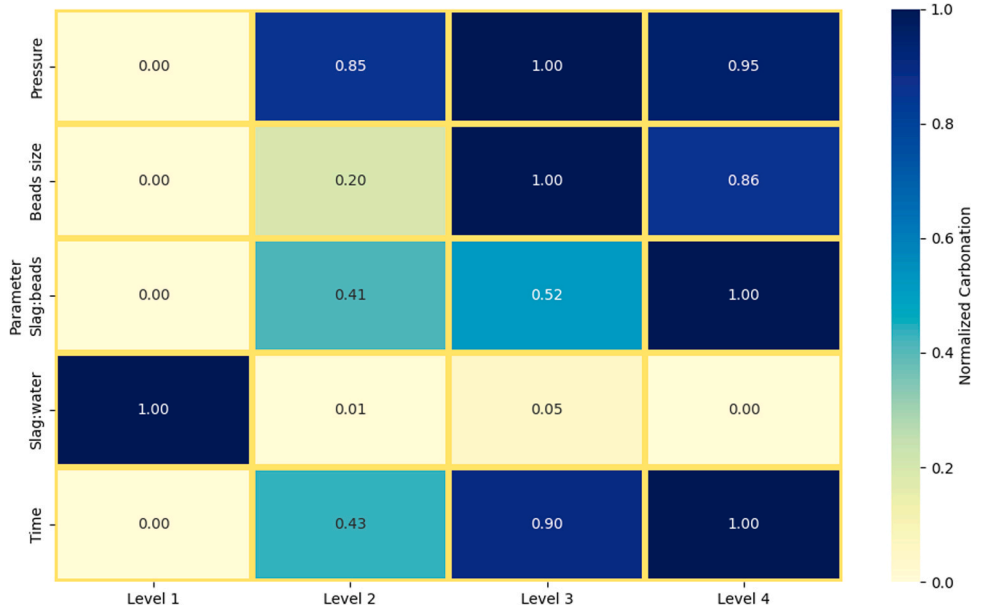



**Fig. 4.** Impact of various parameters on carbonation rate for BOF slag.

will be discussed later. Lastly, the duration of the process is highly influential, as longer times extend the contact time with carbon dioxide. Furthermore, prolonged milling continuously refreshes the surface available for carbonation (Ceyssens et al., 2025). Based on the analysis of Fig. 1, optimal parameters for AOD slag can be estimated as: 5 bar $CO_2$ pressure, 2 mm beads, 1:40 g/g slag-to-bead ratio (B), 1:20 g/g slag-to-water ratio (W), and 8 min of simultaneous milling and carbonation.

Fig. 2 shows slightly different trends for the simultaneous milling and carbonation of BOF slag. It can be seen that pressure plays a significant role up to 2 bar. Above this level, the S/N ratio remains relatively constant. A possible reason is that raw BOF slag is already 47.4% amorphous (Table 2), which limits further amorphisation of the material. Regarding bead size, larger beads (5 mm and 10 mm) perform slightly better compared to smaller beads (2 mm and 3 mm), as the initial mean particle diameter of the BOF slag is 64.5 μm. Similar to AOD slag, increasing the slag-to-bead ratio increases carbon dioxide uptake, but without a clear plateau. The slag-to-water ratio has a minor, almost negligible impact on the carbonation rate of BOF slag. Furthermore, the duration of simultaneous milling and carbonation influences the process for the reasons mentioned earlier. The only notable difference in comparison with AOD slag is the plateau reached after 6 min for BOF slag, most likely because more amorphous material needs less contact time with $CO_2$ to completely react. Based on this, the optimal parameters for BOF slag are estimated as follows: 2 bar $CO_2$ pressure, 5 mm beads, a 1:40 g/g slag-to-bead ratio (B), a 1:5 g/g slag-to-water ratio (W), and a 6-minute process duration. As observed, the optimal parameters for AOD and BOF slags differ significantly, indicating that the process is material-specific, and that for different materials optimal conditions will vary.

**Table 4**
ANOVA contribution of five factors on carbonation rate of AOD and BOF.

| | % contribution | |
|---|---|---|
| Factor | AOD | BOF |
| Pressure | 52 | 41 |
| Beads size | 2 | 4 |
| Slag-to-bead ratio | 3 | 21 |
| Slag-to-water ratio | 2 | 0 |
| Time | 41 | 34 |

### 3.1.2. Heatmaps based on normalised carbonation rate

In order to approve previously estimated optimal parameters, additional analysis of the carbonation rate using heatmaps is conducted. A heatmap is a method for visualising matrix-like data by using colours as the main element (Gu, 2022). This method can provide an overview of the broad patterns in the data sets (Sukumar, 2024). In contrast to the S/N ratio previously described, heatmaps are sensitive to outliers and don't account for noise in the data sets (Sigma Computing, 2025), which allows for an alternative perspective on the same data. Heatmaps for both AOD and BOF are given in Figs. 3 and 4, respectively.

Results obtained by analysing heatmaps gave similar conclusions to those obtained with the S/N ratio. Therefore, the same explanations hold for the influence of the examined factors on the carbonation rate of AOD and BOF. Optimal parameters for both slags are chosen based on the highest normalised carbonation rate. For AOD, these parameters are 5 bar $CO_2$ pressure, 2 mm beads, 1:30 g/g slag-to-bead ratio (B), 1:10 g/g slag-to-water ratio (W) and 8 min. For BOF, optimal parameters are 4 bar $CO_2$ pressure, 5 mm beads, 1:40 g/g slag-to-bead ratio (B), 1:5 g/g slag-to-water (W) ratio and 8 min of simultaneous milling and carbonation.

It can be observed that differences in optimal parameters selected based on S/N ratio and heatmaps occur in two factors for each slag. For AOD slag, there is a discrepancy between slag-to-bead ratio and slag-to-water ratio. Conversely, there is a slight difference between optimal parameters for pressure and time used in the BOF slag process. These discrepancies occur from the evaluation methods, as the S/N ratio provides a trend from which the choice of optimal parameters can be minimised, while heatmaps only analyse the absolute values of the carbonation rate achieved and propose the best possible outcome without accounting for noise. In order to determine the significance of each factor in the process of simultaneous milling and carbonation, ANOVA analysis for the contribution of each factor is performed.

### 3.1.3. ANOVA contribution of each factor

The relative importance of controlling factors can be quantified using ANOVA. This analysis yielded p-values of 0.04 and 0.004, and F-factors of 3.6 and 7.65 for AOD and BOF, respectively. To further interpret these results, the contribution of each factor was calculated.

The variability explained by each factor is measured through its sum of squares (SS) and the percent contribution is expressed as a ratio of each factor's SS and total SS (Mustapha et al., 2021). The contribution of all five examined factors is shown in Table 4.

It is important to emphasise that all examined parameters contribute to the process of simultaneous milling and carbonation, as this system is rather complex. Nevertheless, changes in parameters with the highest percentage contribution cause the greatest change in carbonation rates. From Table 4, it can be observed that changes in pressure and time have the biggest contribution to this process, as previously discussed. However, a notable difference in the contribution of slag-to-bead ratio can be seen for AOD and BOF slag. This variation can be attributed to differences in their chemical composition. As shown in Table 1, BOF slag contains a substantially higher percentage of iron compared to AOD slag. The higher iron content makes BOF slag a coarser material, thereby increasing the importance of the slag-to-bead ratio, specifically, the frequency of collisions between the beads and slag particles, in enhancing the effectiveness of the milling and carbonation process.

## 3.2. Optimal parameters for simultaneous milling and carbonation

The carbonation rates of the optimal parameters previously estimated for AOD and BOF are given in Figs. 5a and 5b, respectively. Grey bars represent optimal parameters estimated by the S/N ratio method, while blue bars represent optimal parameters estimated by heatmaps. Error bars reflect variability across three repetitions. Carbonation rates achieved by both methods were 0.32 g of $CO_2$/g of AOD slag and 0.25 g of $CO_2$/g of BOF slag.

As seen in Fig. 5, both AOD and BOF achieved slightly better carbonation rates with the estimation of heatmaps. However, it can be

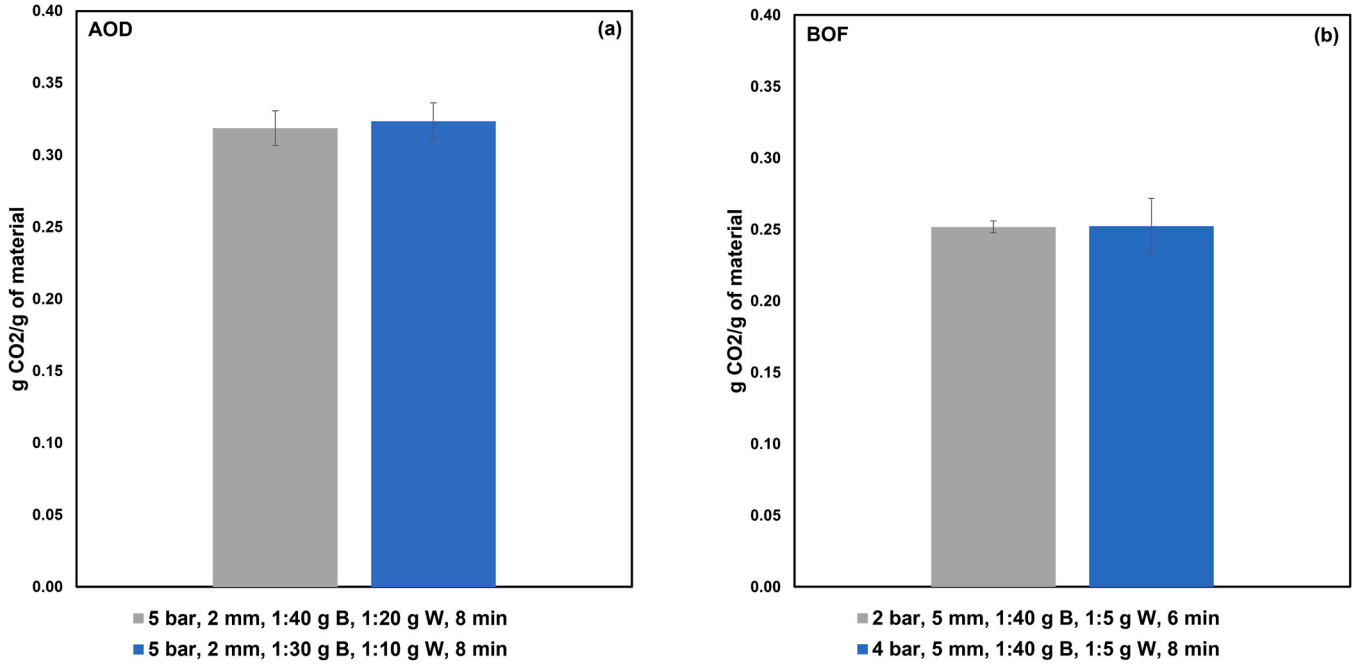



**Fig. 5.** Carbonation rate for (a) AOD and (b) BOF at optimal parameters previously estimated.

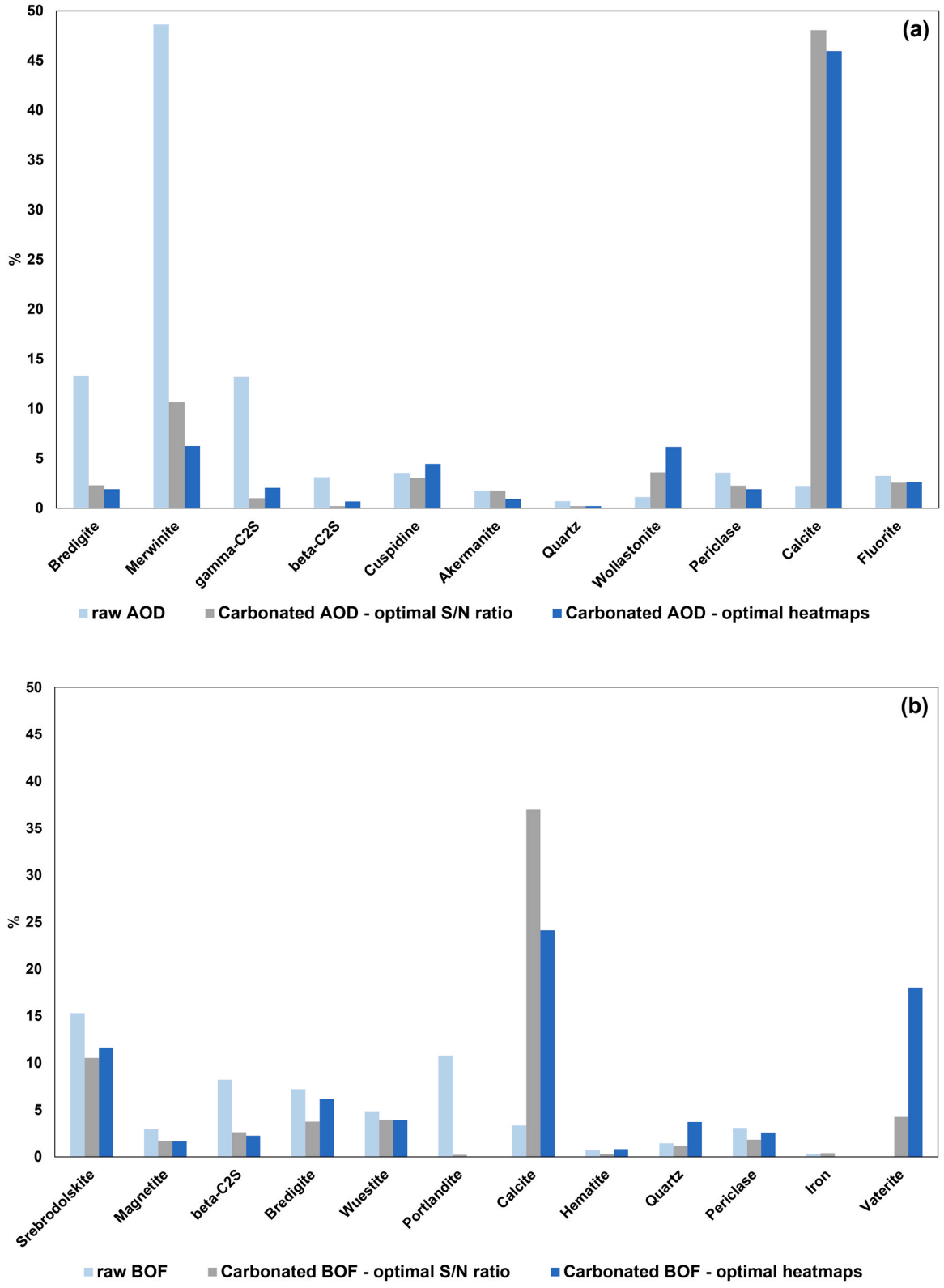



**Fig. 6.** Mineral composition of (a) raw AOD and carbonated AOD at optimal parameters and (b) raw BOF and carbonated BOF at optimal parameters.

observed that these differences are within the margin of error. Given the overarching objective of minimising input parameters to maximise the carbonation rate, it can be concluded that the optimal minimal conditions for AOD slag were determined based on heatmap estimations (5 bar $CO_2$ pressure, 2 mm beads, 1:30 g/g slag-to-bead ratio (B), 1:10 g/g slag-to-water ratio (W), and 8 min). In contrast, for BOF slag, the minimal optimal parameters were identified using the signal-to-noise (S/N) ratio analysis (2 bar $CO_2$ pressure, 5 mm beads, a 1:40 g/g slag-to-bead ratio (B), a 1:5 g/g slag-to-water ratio (W), and 6 min). Impact energy calculated at these parameters, using Eq. 11, for AOD was 110 J/g, while for BOF it was 152 J/g. A detailed environmental and economic assessment of this process, including the implemented energy

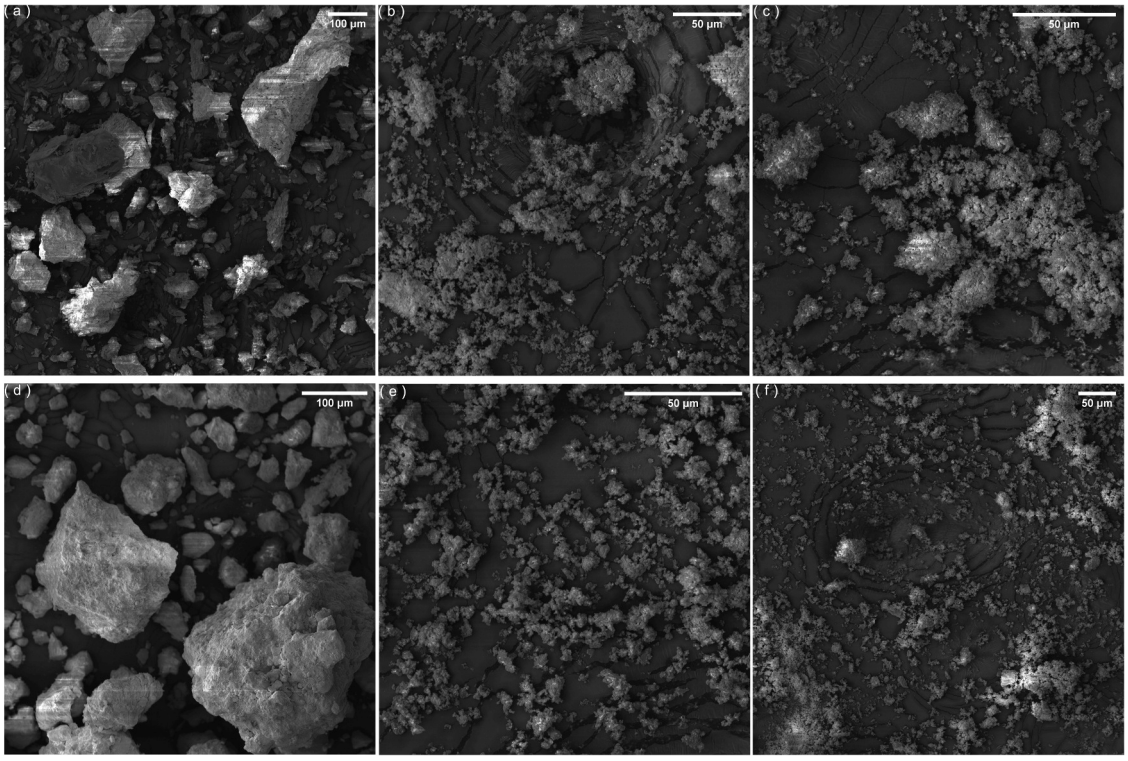



**Fig. 7.** Representative SEM micrographs of (a) raw AOD, (b) carbonated AOD optimisation with S/N ratio, (c) carbonated AOD optimisation with heatmaps, (d) raw BOF, (e) carbonated BOF optimisation with S/N ratio, (f) carbonated BOF optimisation with heatmaps.

requirements, can be found in the study by Watjanatepin et al (Watjanatepin et al., 2024).

Considering the mineral composition of AOD and BOF slags, changes in mineral phases detected by XRD are given in Figs. 6a and 6b. The numerical values for carbonated samples are given in Supplementary data Table 3, and XRD patterns in Supplementary data Fig. 2.

From Fig. 6a, it is evident that amounts of bredigite, merwinite, γ-$C_2S$ and β-$C_2S$ significantly decreased after simultaneous milling and carbonation, indicating their high reactivity (Mo et al., 2025). Due to the nature of these minerals, they likely carbonate via reactions given with Eqs. 12–17 (Mirhadi et al., 2012; Liu et al., 2024a). Bredigite may decompose into $C_2S$ and merwinite (Eq. 12), after which merwinite undergoes further dissolution to $C_2S$ and magnesium silicate (Eq. 13). Subsequently, $C_2S$ may transform into wollastonite and lime (Eq. 14). The dissolution products generated from these reactions then react with hydrogencarbonate, ultimately forming carbonates as the final products (Eqs. 15–17).

$$Ca_7Mg(SiO_4)_{4\ (s)} \rightarrow 2Ca_2SiO_{4(aq)} + Ca_3Mg(SiO_4)_{2\ (aq)} \quad (12)$$

$$3Ca_3Mg(SiO_4)_{2\ (s)} \rightarrow 2Ca_2SiO_{4(aq)} + 3MgSiO_{3(aq)} + SiO_{2(s)} + 5CaO_{(aq)} \quad (13)$$

$$Ca_2SiO_{4(s)} \rightarrow CaSiO_{3(s)} + CaO_{(aq)} \quad (14)$$

$$Ca_2SiO_{4(s)} + 2HCO^-_{3(aq)} \rightarrow 2CaCO_{3(s)} + SiO_{2(s)} + 2OH^-_{(aq)} \quad (15)$$

$$Ca(Mg)SiO_{3(s)} + HCO^-_{3(aq)} \rightarrow Ca(Mg)CO_{3(s)} + SiO_{2(s)} + OH^-_{(aq)} \quad (16)$$

$$CaO_{(aq)} + CO_{2(aq)} \rightarrow CaCO_{3(s)} \quad (17)$$

In contrast, phases such as cuspidine, akermanite, quartz, periclase, and fluorite exhibited minimal or no change, suggesting that they are only slightly or non-reactive during the carbonation process. Notably, the contents of wollastonite and calcite increased as a direct consequence of carbonation. Based on XRD analysis, the amount of $CO_2$ captured in crystalline form was calculated to be 0.27 g of $CO_2$/g of material for optimal conditions estimated with the S/N ratio method, and 0.25 g of $CO_2$/g of material based on heatmaps estimation.

The mineralogy of BOF slag differs from that of AOD slag. However, as shown in Fig. 6b, significant reductions were observed in mineral phases such as srebrodolskite, β-$C_2S$ and portlandite, aligning with previous findings in the literature (Zhou et al., 2025; Ismail et al., 2016). The dissolution of srebrodolskite is shown in Eq. 18, while the dissolution of $C_2S$ and its reaction with hydrogencarbonate are presented in Eqs. 19 and 20. The reactions involving the formed lime and the existing portlandite are illustrated in Eq. 21 and 22.

$$Ca_2Fe_2O_{5\ (s)} \rightarrow 2CaO_{(aq)} + Fe_2O_{3(aq)} \quad (18)$$

$$Ca_2SiO_{4(s)} \rightarrow CaSiO_{3(s)} + CaO_{(aq)} \quad (19)$$

$$Ca_2SiO_{4(s)} + 2HCO^-_{3(aq)} \rightarrow 2CaCO_{3(s)} + SiO_{2(s)} + 2OH^-_{(aq)} \quad (20)$$

$$CaO_{(aq)} + CO_{2(aq)} \rightarrow CaCO_{3(s)} \quad (21)$$

$$Ca(OH)_{2(s)} + CO_{2(aq)} \rightarrow CaCO_{3(s)} + H_2O_{(l)} \quad (22)$$

Conversely, minimal or no decreases were noted for magnetite, bredigite, wuestite, haematite, quartz, periclase and iron content. Importantly, an increase in the amounts of calcite and vaterite can be observed. A notable distinction between the two sets of optimal conditions lies in the amount of vaterite formed. At optimal conditions estimated with heatmaps (4 bar pressure), higher content of vaterite was observed compared to conditions estimated with analysis of S/N ratio (2 bar pressure). While the total amount of carbonates formed was similar, the applied conditions influenced the dominant calcium carbonate polymorph formed. The calculated $CO_2$ captured in crystalline form was 0.22 g of $CO_2$/g of material for S/N ratio estimation and 0.23 g of $CO_2$/g of material for heatmaps estimation.

SEM micrographs of the raw and carbonated slags are shown in Fig. 7. A notable reduction in particle size is observed after simultaneous

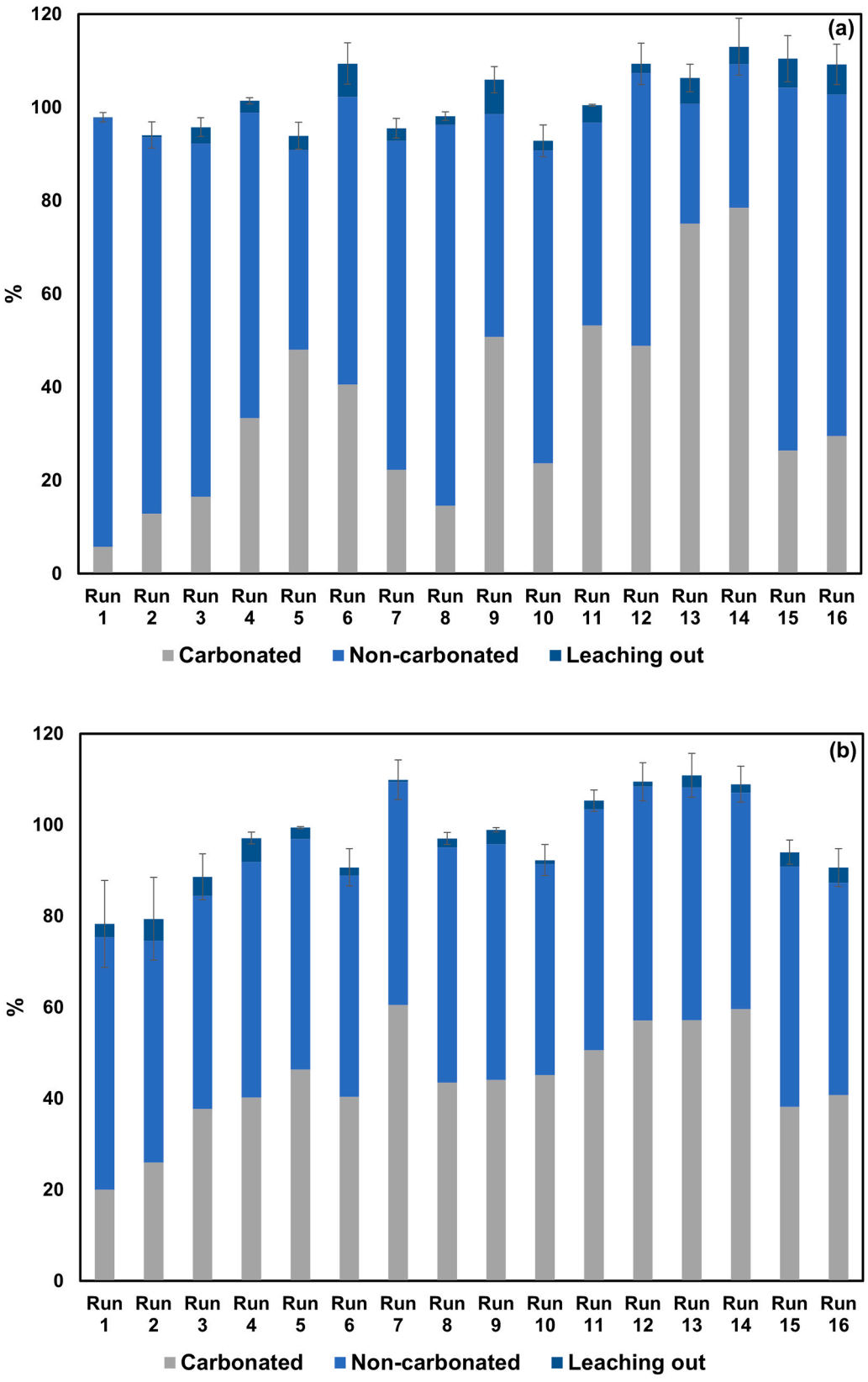



**Fig. 8.** Ca/Mg mass balance for (a) AOD and (b) BOF for all conducted experiments.

milling and carbonation. Moreover, the carbonated particles exhibit smoother surfaces compared to the raw particles, along with more pronounced inter-particle voids and reduced density, attributable to increased porosity. However, no significant differences in particle morphology are evident between the two optimisation methods for milling and carbonation conditions.

### 3.3. Impact of varied parameters on metal leaching in the water

Planetary ball milling is a milling technique used to grind materials into very fine powders (Burmeister and Kwade, 2013) and prompt specific chemical reactions (Bolm and Hernandez, 2019). Accordingly, the method has been widely used for the leaching of a variety of elements from different matrices, such as indium and tin from waste (Qin et al., 2021), heavy metals from fly ash (Chen et al., 2016) and calcium from the rare earth concentrate (Liu et al., 2024b). Therefore, an examination of elements leached into the water during the Taguchi design runs was conducted using ICP-OES. It was observed that only calcium and magnesium leached out. In addition to calcium and magnesium, also chromium, barium, aluminium, lithium, lead, nickel, iron, copper, cobalt and zinc were measured, but these remained under the detection limit of 10 ppm. Therefore, the mass balance of calcium and magnesium is presented in Figs. 8a and 8b for AOD and BOF, respectively. These results are obtained using XRD to quantify the carbonated fraction, XRF to determine the total elemental composition, and ICP-OES to measure the concentration of ions in the solution. The results indicate that AOD slag leaches out up to 4% of the total calcium and magnesium content. As the leachate exhibited a milky-white appearance, the solution was dried, resulting in a white solid residue for further analysis. SEM-EDX was employed to characterise this residual powder and to identify the solid forms in which the leached species were present in the aqueous phase (Supplementary data Fig. 3). It was observed that the leached content was primarily present in the form of silicates, carbonates and silica. These observations were complemented with ICP-OES measurements. In comparison, BOF slag leaches out up to 2% of these elements in a similar form. Overall, the leaching values fall within the experimental error range. Additionally, a substantial proportion of non-carbonated calcium and magnesium remains in both slags. XRD analysis reveals that these non-carbonated elements are predominantly associated with wollastonite and merwinite in AOD slag and srebrodolskite and β-$C_2S$ in BOF slag, indicating limitations of achieving complete carbonation of these slags.

### 3.4. Influence of particle size on $CO_2$ uptake

Given the complexity of a system in which slags are simultaneously milled and carbonated, an attempt is made to estimate the influence of particle size on $CO_2$ uptake. Trends of S/N ratio for breakage of particles and carbonation rate are given in Supplementary Data Figs. 4a and 4b. It was observed that the D50 value of AOD slag abruptly increased in most cases (therefore, breakage potential decreased) with the increase of carbonation rate, suggesting that AOD slag tends to agglomerate with the carbonation process (Miladinović et al., 2025). On the other hand, particle breakage in BOF slag followed the trend of carbonation, indicating that the carbonation process in BOF slag is primarily influenced by particle size, i.e. smaller particles tend to carbonate more effectively. However, observed trends are not consistent for all parameters and further research is needed.

## 4. Conclusion

In order to maximise $CO_2$ uptake of Basic Oxygen Furnace (BOF) and Argon Oxygen Decarburisation (AOD) slags, a process combining mechanical activation and carbonation within a planetary ball mill was employed. Five different parameters (pressure of $CO_2$ injected, bead size of milling media, slag-to-bead ratio, slag-to-water ratio and time of the process) at four different levels were examined. A Taguchi design of experiment was used to minimise the number of experimental runs. The results were analysed using both signal-to-noise (S/N) ratio and heatmaps visualisations to identify optimal conditions for maximal $CO_2$ uptake. Both optimisation approaches yielded similar carbonation efficiencies. However, the optimal parameters for minimising their usage in AOD slag were determined based on heatmap estimations (5 bar $CO_2$ pressure, 2 mm beads, 1:30 g/g slag-to-bead ratio (B), 1:10 g/g slag-to-water ratio (W), and 8 min). In contrast, for BOF slag, the minimal optimal parameters were identified using the signal-to-noise (S/N) ratio analysis (2 bar $CO_2$ pressure, 5 mm beads, a 1:40 g/g slag-to-bead ratio (B), a 1:5 g/g slag-to-water ratio (W), and 6 min). These differences are attributed to the distinct material characteristics of each slag, such as mineralogy and particle size. The corresponding $CO_2$ uptake rates under these optimised conditions were 0.32 g $CO_2$/g material for AOD slag and 0.25 g $CO_2$/g material for BOF slag. These rates match or exceed values found in the literature. Notably, the simultaneous milling and carbonation process lasted only 6–8 min, a significant improvement over traditional methods requiring at least 60 min. This demonstrates that mechanical activation substantially enhances the carbonation rate through the forces applied during milling. Furthermore, no leaching of metals other than calcium and magnesium was observed. The impact energies applied were 110 J/g for AOD and 152 J/g for BOF, supporting efficient activation and carbonation without undesirable side effects.

## Funding

This work was supported by The Research Foundation – Flanders (FWO) within the AgriCarb project (G0A4821N) and C-farms project (S004023N).

## CRediT authorship contribution statement

**Giuseppe Granata:** Writing – review & editing, Supervision. **Luka Ceyssens:** Writing – review & editing, Validation, Methodology, Investigation. **Tom Van Gerven:** Writing – review & editing, Supervision, Resources, Project administration, Methodology, Funding acquisition, Conceptualization. **Nina Miladinović:** Writing – original draft, Visualization, Validation, Methodology, Investigation, Formal analysis, Conceptualization.

## Declaration of Competing Interest

The authors declare that they have no known competing financial interests or personal relationships that could have appeared to influence the work reported in this paper.

## Appendix A. Supporting information

Supplementary data associated with this article can be found in the online version at doi:10.1016/j.cherd.2026.02.058.

## References

Arora, A.K., 2000. Pressure-induced amorphization versus decomposition. Solid State Commun. 115 (12), 665–668.
Bernoux, M., Feller, C., Cerri, C.C., Eschenbrenner, V., Cerri, C.E.P., 2005. Soil carbon sequestration. Soil Erosion and Carbon Dynamics. CRC Press, Boca Raton, pp. 1–24.
Biava, G., Depero, L.E., Bontempi, E., 2024. Accelerated carbonation of steel slag and their valorisation in cement products: a review. Span. J. Soil Sci. 14.
Bolm, C., Hernandez, J.G., 2019. Mechanochemistry of gaseous reactants. Chem. A Eur. J. 58.
Burmeister, C.F., Kwade, A., 2013. Process engineering with planetary ball mills. Chem. Soc. Rev. 42.
Castellote, M., Andrade, C., 2008. Modelling the carbonation of cementitious matrices by means of the unreacted-core model (UR-CORE). Cem. Concr. Res. 38 (12), 1374–1384.
Ceyssens, L., Miladinović, N., Granata, G., Van Gerven, T., 2025. Mechanochemical activation of argon oxygen decarburization slags for improved mineral carbonation. Chem. Eng. & Technol. 48.
Chalouati, S., Yoosefdoost, A., Wai Chiang, Y., Santos, R.M., 2023. Intensified mineral carbonation of natural Canadian silicates using simultaneous ball milling. Int. J. Coal Geol. 277, 104332.
Chen, Z., Cang, Z., Yang, F., Zhang, J., Zhang, L., 2021. Carbonation of steelmaking slag presents an opportunity for carbon neutrality: a review. J. $CO_2$ Util. 54, 101738.
Chen, Z., Lu, S., Mao, Q., Buekens, A., Chang, W., Wang, X., Yan, J., 2016. Suppressing heavy metal leaching through ball milling of fly ash. Energy Waste Manag. 9, 524.
Cui, X.Y., Ringer, S.P., Wang, G., Stachurski, Z.H., 2019. What should the density of amorphous solids be? J. Chem. Phys. 151, 194506.

De Schutter, A., Ceyssens, L., Granata, G., Van Gerven, T., 2024. Improving the carbonation of steel slags through concurrent wet milling. J. Sustain. Metall. 10, 1759–1773.
Dhoble, Y.N., Ahmed, S., 2018. Review on the innovative uses of steel slag for waste minimization. J. Mater. Cycles Waste Manag. 20, 1373–1382.
Digiovanni, C., Hisseine, O.A., Awolayo, A.N., 2024. Carbon dioxide sequestration through steel slag carbonation: review of mechanisms, process parameters, and cleaner upcycling pathways. J. $CO_2$ Util. 81, 102738.
Goodbrake, C.J., Young, J.F., Berger, R.L., 1979. Reaction of hydraulic calcium silicates with carbon dioxide and water. J. Am. Ceram. Soc. 62 (9–10), 488–491.
Gu, Z., 2022. Complex heatmap visualization. iMeta 1.
Hisam, M.W., Dar, A.A., Elrasheed, M.O., Khan, M.S., Gera, R., Azad, I., 2024. The versatility of the Taguchi method. J. Stat. Theory Appl. 23, 365–389.
Ismail, M., Liu, W., Chan, M.S.C., Dunstan, M.T., Scott, S.A., 2016. Synthesis, application, and carbonation behavior of $Ca_2Fe_2O_5$ for chemical looping hydrogen production. Energy & Fuels 30, 6220–6232.
Jafter, O.F., Lee, S., Park, J., Cabanetos, C., Lungerich, D., 2024. Navigating ball mill specifications for theory-to-practice reproducibility in mechanochemistry. Angew. Chem. Int. Ed. 63.
Jat, M.L., Chakraborty, D., Ladha, J.K., Parihar, C.M., Datta, A., Mandal, B., Nayak, H.S., Maity, P., Rana, D.S., Chaudhari, S.K., Gerard, B., 2022. Carbon sequestration potential, challenges, and strategies towards climate action in smallholder agricultural systems of South Asia. Crop Environ. 1, 86–101.
Joint Research Centre (European Commission). EU climate targets: how to decarbonise the steel industry [online]. 2022. Available from: ⟨https://joint-research-centre.ec.europa.eu/jrc-news-and-updates/eu-climate-targets-how-decarbonise-steel-industry-2022-06-15_en⟩ [Accessed 17 June 2025].
Khoa, H.X., Bae, S., Bae, S., Kim, B., Kim, J.S., 2004. Planetary ball mill process in aspect of milling energy. J. Powder Mater. 21 (2), 155–164.
Kim, E., Spooren, J., Broos, K., Nielsen, P., Horckmans, L., Vrancken, K.C., Quaghebeur, M., 2016. New method for selective Cr recovery from stainless steel slag by NaOCl-assisted alkaline leaching and consecutive $BaCrO_4$ precipitation. Chem. Eng. J. 295, 542–551.
Kremer, D., Dertmann, C., Etzold, S., Telle, R., Friedrich, B., Wortuba, H., 2022. Ex-situ mineral carbonation – a parameter study on carbon mineralisation in an autoclave. J. $CO_2$ Util. 58, 101928.
Krivsky, W.A., 1973. The Linde argon-oxygen process for stainless steel: a case study of major innovation in a basic industry. Metall. Trans. 4, 1439–1446.
Liu, J., Chen, B., Feng, Y., Cao, Y., Huang, Y., Shi, Y., M, 2024b. Selective leaching of calcium from mechanically activated mixed rare earth concentrate. J. Rare Earths 42.
Liu, S., Rong, P., Zhang, S., Guo, H., Guan, X., Zhu, J., Mi, T., 2024a. Enhancing $CO_2$-cured cementitious binder with Mg-doped $\gamma$-$C_2S$ from high-Mg limestone. Dev. Built Environ. 17.
Madu, I.E., Madu, C.N., 1999. Design optimization using signal-to-noise ratio. Simul. Pract. Theory 7 (4), 349–372.
Magini, M., Colella, C., Iasonna, A., Padella, F., 1998. Power measurements during mechanical milling—II. Acta Mater. 46 (8), 2841–2850.
Miladinović, N., Ceyssens, L., Granata, G., Van Gerven, T., 2025. Impact of particle breakage on the carbonation of argon oxygen decarburization slag. J. $CO_2$ Util. 95, 103073.
Mirhadi, S.M., Tavangarian, F., Emadi, R., 2012. Synthesis, characterization and formation mechanism of single-phase nanostructured bredigite powder. Mater. Sci. Eng. 32.
Mitra, A., 2011. The Taguchi method. WIREs Comput. Stat. 3 (5), 472–480.
Mo, L., Liu, P., Gu, Y., Kuang, J., 2025. Transforming AOD slag toward a highly reactive mineral admixture with appreciable $CO_2$ sequestration. Cem. Concr. Compos. 156, 105863.
Morsi, H., Yong, K.L., Jewell, A.P., 2004. Evaluation of the Taguchi methods for the simultaneous assessment of multiple variables in the tumour microenvironment. Int. Semin. Surg. Oncol.
Mustapha, A.N., Zhang, Y., Zhang, Z., Ding, Y., Yuan, Q., Li, Y., 2021. Taguchi and ANOVA analysis for the optimization of microencapsulation of a volatile phase change material. J. Mater. Res. Technol. 11.
Odebiyi, O.S., Guo, Y., Du, H., Liu, B., Wang, S., 2024. Effect of mechanochemical activation parameters on vanadium recovery from steel slag. Mater. Chem. Phys. 324, 129697.
Paneva, M., Stoimenov, N., Panev, P., 2024. Methodology for experimental determination of a ball mill critical speed. AIP Conf. Proc.
Pohshna, C., Mailapalli, D.R., 2023. Modeling the particle size of nanomaterials synthesized in a planetary ball mill. OpenNano 14, 100191.
Qin, J., Ning, S., Fujita, T., Wei, Y., Zhang, S., Lu, S., 2021. Leaching of indium and tin from waste LCD by a time-efficient method assisted planetary high-energy ball milling. Waste Manag. 120, 193–201.
Radune, M., Lugovskoy, S., Knop, Y., Yankelevitch, A., 2022. Use of Taguchi method for high-energy ball milling of $CaCO_3$. J. Mater. Sci. Mater. Eng. 17.
Rashid, K.M.J., 2023. Optimize the Taguchi method, the signal-to-noise ratio, and the sensitivity. Int. J. Stat. Appl. Math. 8 (6), 64–70.
Ruth, M., 2004. Steel production and energy. Encyclopedia of Energy. Elsevier, Amsterdam, pp. 695–706.
Santos, R.M., Van Bouwel, J., Vandevelde, E., Mertens, G., Elsen, J., Van Gerven, T., 2013. Accelerated mineral carbonation of stainless steel slags for $CO_2$ storage and waste valorization. Int. J. Greenh. Gas. Control 17, 32–45.
Sigma Computing. Heatmaps 101: numbers to insight in one glance [online]. 2025. Available from: ⟨https://www.sigmacomputing.com/blog/heatmaps⟩ [Accessed 18 August 2025].
Ståhle, L., Wold, S., 1989. Analysis of variance (ANOVA). Chemom. Intell. Lab. Syst. 6 (4), 259–272.
Sukumar, H. Heatmaps in data visualization: a comprehensive introduction [online]. 2024. Available from: ⟨https://inforiver.com/insights/heatmaps-in-data-visualization-a-comprehensive-introduction/⟩ [Accessed 18 August 2025].
Ukwattage, N.L., Ranjith, P.G.R., Li, X., 2017. Steel-making slag for mineral sequestration of carbon dioxide by accelerated carbonation. Measurement 97, 15–22.
University Of York. Orthogonal arrays (Taguchi designs) [online]. 2004. Available from: ⟨https://www.york.ac.uk/depts/maths/tables/orthogonal.htm⟩ [Accessed 19 June 2025].
Wang, H., Zhou, G., Mu, Y., Zhang, M., Guo, M., 2024. Enhanced carbon dioxide sequestration and Cr detoxification: direct carbonation of AOD slag with additives under ambient conditions. J. Clean. Prod. 443, 141181.
Watjanatepin, P., Steinwidder, L., De Schutter, A., Miladinović, N., Granata, G., Vicca, S., Van Gerven, T., Van Acker, K., 2024. Preliminary environmental and economic assessment of mineral carbonation of steel slags. Procedia CIRP 122.
Wei, W., Gustavsson, J., Samuelsson, P.B., Gyllenram, R., Tilliander, A., Jonsson, P.G., 2022. Prediction of nitrogen behaviour in the AOD process by a time-dependent thermodynamic model. Ironmak. & Steelmak. 49 (1), 70–82.
World Steel Association. Steel industry co-products [online]. 2021. Available from: ⟨https://worldsteel.org/wp-content/uploads/Fact-sheet-Steel-industry-co-products.pdf⟩ [Accessed 17 June 2025].
World Steel Association. Raw materials [online]. Available from: ⟨https://worldsteel.org/other-topics/raw-materials/⟩ [Accessed 17 June 2025].
Xu, S., Xiao, F., Amirkhanian, S., Singh, D., 2017. Moisture characteristics of mixtures with warm mix asphalt technologies – a review. Constr. Build. Mater. 142, 148–161.
Zhang, Y., Ling, T.C., 2020. Reactivity activation of waste coal gangue and its impact on the properties of cement-based materials – a review. Constr. Build. Mater. 234, 117424.
Zhao, Q., Liu, C., Mei, X., Saxen, H., Zevenhoven, R., 2025. Research progress of steel slag-based carbon sequestration. Fundam. Res. 5, 282–287.
Zhou, G., Wang, H., Zhang, M., Guo, M., 2025. Deciphering the reactivity of specific phases in metallurgical slag under direct wet carbonation conditions. J. Environ. Chem. Eng. 13, 116307.
Z-Mixer. Bead mill grinding in chemicals [online]. 2025. Available from: ⟨https://z-mixer.com/bead-mill-grinding-in-chemicals-unlock-grind-mastery/⟩ [Accessed 18 August 2025].